

Improving Image-Based Localization with Deep Learning: The Impact of the Loss Function

Isaac Ronald Ward, M. A. Asim K. Jalwana and Mohammed Bennamoun

University of Western Australia, Perth, Australia

isaacronaldward@gmail.com,

mohammad.jalwana@research.uwa.edu.au,

mohammed.bennamoun@uwa.edu.au

Abstract

This work formulates a novel loss term which can be appended to an RGB only image localization network’s loss function to improve its performance. A common technique used when regressing a camera’s pose from an image is to formulate the loss as a linear combination of positional and rotational error (using tuned hyperparameters as coefficients). In this work we observe that changes to rotation and position mutually affect the captured image, and in order to improve performance, a network’s loss function should include a term which combines error in both position and rotation. To that end we design a geometric loss term which considers the similarity between the predicted and ground truth poses using both position and rotation, and use it to augment the existing image localization network PoseNet. The loss term is simply appended to the loss function of the already existing image localization network. We achieve improvements in the localization accuracy of the network for indoor scenes: with decreases of up to 9.64% and 2.99% in the median positional and rotational error when compared to similar pipelines.

1 Introduction

The problem of image localization — that is; extracting the position and rotation of the camera with respect to a scene’s coordinate system, directly from a given image (known as a query image) — has been approached using a variety of traditional and deep learning based techniques in the recent years. The problem remains important to solve since it lies at the heart of numerous technologies in computer vision and robotics, e.g. robotic navigation, geo-tagging and augmented reality.

More colloquially, the problem can be understood as trying to find out where you are and where you are looking by considering only the information present in an RGB image.

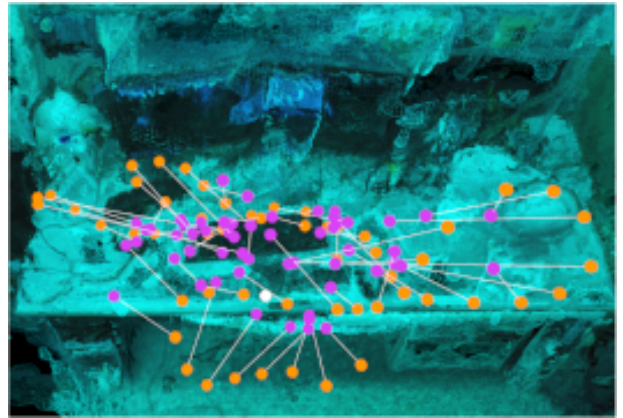


Figure 1: A sample of the predicted pose positions (purple) generated for the ground truth poses (orange) in the 7Scenes *Heads* scene using our proposed model. The scene’s origin (white) and SfM reconstruction is rendered for reference. Note the correlation between the predictions and ground truth values, especially when compared to Figure 3. Image best viewed in color.

In the literature this is sometimes referred to as **the kidnapped robot problem**: “how can a device re-localize itself with any certainty from an arbitrary, unknown location”. Since a camera is capturing the input image, the terms image localization and camera (re)localization are often used interchangeably. Pipelines which localize from image inputs only can also be referred to as Visual Positioning Systems (VPS).

Convolutional neural network (CNN) based approaches to image localization — such as PoseNet [4] — have found success in the recent years due to the availability of large datasets and powerful training hardware, but the performance gap between these systems and the more accurate SIFT feature-based pipelines remains large. The SIFT-based Active Search algorithm [12] for example remains as a reminder that significant improvements need to be made be-

fore CNN techniques can be considered competitive in the image localization task.

However, CNN-based approaches do possess number of characteristics which qualify them for robustly handling the camera relocalization task. Namely, CNNs are robust to changes in illumination and occlusion within an environment [9], they can operate in close to real time [7] (~ 30 frames per second) and can be trained from labelled data (which can easily be gathered via structure from motion for any arbitrary scene [14, 13]). CNN based systems also tend to excel in textureless environments and in other cases where SIFT based methods would typically fail [1]. They are also proven to operate well using only simple RGB data — making them an ideal solution for navigation in simple, cheap robotic devices such as drones and unmanned ground vehicles. Extending existing pipelines whilst preserving these benefits is important for solving the image localization problem in this context.

A key observation when considering existing CNN approaches is how position and rotation (herein referred to as the ‘pose’) are treated separately. It can be observed that altering a camera’s position *or* rotation both affect the image produced, and hence the error in the regressed position and the regressed rotation cannot be decoupled — each mutually affects the other. In order to optimize a network for regressing a camera’s pose accurately, a loss term should be used which combines both distinct quantities in a more intuitive fashion than Euclidean distance measures.

This publication thus offers the following key contributions:

1. The formulation of a loss term which considers the error in both the regressed position and rotation in its calculation (Section 3).
2. Evaluation of a network augmented with this loss term and a comparison of its performance with state-of-the-art image localization methods (Section 5).

2 Related work

Perhaps the most relevant work to this proposed work is the PoseNet camera pose regression network [4]. The PoseNet architecture is one of the first CNNs to regress the 6 degrees of freedom in a camera’s pose. The network is pretrained on object detection datasets in order to maximize the quality of feature extraction, which occurs in the first stage of the network. It only requires a single RGB image as input, requiring no auxiliary input unlike other networks [18, 11], and operates in real time, making it ideal for time sensitive contexts such as drone navigation.

Notably, PoseNet is able to localize images in hard conditions — specifically in areas with large textureless surfaces

where SIFT-based traditional methods fail. PoseNet’s end-to-end nature and relatively simple ‘one-step’ training process makes it perfect for the purpose of testing under augmentation (altering or modifying the network — in this case by changing its loss function).

PoseNet notably had its loss function augmented in [3] where it was demonstrated that changing a pose regression network’s loss function is sufficient enough to cause an improvement in performance. The network was similarly ‘upgraded’ in [19] using LSTMs to correlate features at the CNNs output. Additional improvements to the network were completed in [2], where a Bayesian CNN implementation was used to estimate relocalization accuracy.

More complex CNN approaches do exist [9, 8, 10]. The pipeline outlined in [5] for example uses a CNN to regress the relative poses between a set of images which are *similar* to a query image. These relative pose estimates are coalesced in a fusion algorithm which produces an estimate for the camera pose of the query image.

Often depth data is incorporated in order to leverage the information encoded in multi-modal inputs. These RGB-D input pipelines are commonplace in the image localization literature [1], and typically boast higher localization accuracy at the cost of requiring additional sensors and data.

A variety of non-neural network solutions exist, with one of the more notable solutions being the Active Search algorithm [12], which uses SIFT features to inform a matching process. SIFT descriptors are calculated over the query image and are directly compared to a known 3D model’s SIFT features. SIFT and other non CNN learned descriptors have been used to achieve high localization accuracy, but these descriptors tend to be susceptible to changes in the environment, and the systems which use them often have a higher memory and computational cost. As such, CNN-based methods are the primary focus of this work.

3 The proposed loss term

The motivation behind the first part of our loss term’s design is to ensure that the predicted pose is indeed always ‘looking’ in the right direction. We begin by considering the transformation from world coordinates $[\mathbf{W}]$ to image coordinates $[\mathbf{I}]$ using a calibration matrix $[\mathbf{K}]$, a translation represented by the 3-vector $\vec{\mathbf{t}}$ and a rotation defined by a rotation matrix $[\mathbf{R}]$ as per Equation (1).

$$[\mathbf{I}] = [\mathbf{K}][\mathbf{R} ; \vec{\mathbf{t}}][\mathbf{W}] \quad (1)$$

Naturally we can instead convert to camera coordinates $[\mathbf{C}]$, as in Equation (2), if we are without the camera calibration matrix.

$$[\mathbf{C}] = [\mathbf{R} ; \vec{\mathbf{t}}][\mathbf{W}] \quad (2)$$

Transforming from world to camera coordinates can thus be accomplished easily, and from there the poses at each camera position can be extracted. Herein lies the problem; in the camera’s coordinate system, the centre of the camera lies at the origin. This extends to any camera coordinate system calculated in this way, meaning that the quantities of interest cannot be directly compared, as they do not share a common coordinate system.

The world coordinate system is however fixed for all cameras, and multiple ‘cameras’ (or a single camera in different poses) can be compared in this coordinates system once transformed (Equation (3)).

$$[\mathbf{W}] = [\mathbf{R} \mid \vec{\mathbf{t}}]^{-1}[\mathbf{C}] \quad (3)$$

More explicitly, since the camera is by convention always facing in the negative z-direction, a vector representing it’s direction in world space can be calculated as per Equation (4). This vector is calculated with respect to world coordinates and can thus be used for comparison across different camera positions.

$$p = [\mathbf{R} \mid \vec{\mathbf{t}}]^{-1} [0 \ 0 \ -1]^T \quad (4)$$

We can use this method (Equation (4)) to calculate a pose vector given values of $[\mathbf{R}]$ and $\vec{\mathbf{t}}$. Hence, pose vectors for the ground truth and for predictions can be calculated easily (provided we know the translation and rotation of the pose). Maximizing the similarity between such vectors ensures that one is facing in the correct direction, and that the prediction is aligned with the ground truth.

A loss term can then be formulated which combines both translational and rotational error by considering the difference between the predicted and ground truth position vectors, which we term the **delta** vector, see Figure 2. The cosine similarity between the delta vector and the ground truth position vector — rather than the difference between the ground truth position vector and the predicted position vector — is used as a measure of similarity.

A loss term designed in this way ensures that the network, at a high level, considers both position and rotation when regressing pose from an image.

3.1 Calculating the proposed loss term

The final and most successful geometric loss term (termed \mathcal{L}_{geo}) used to gather results for this work is as outlined in Equation (7). Where $\vec{\mathbf{d}}$, the delta vector and \bar{s} , the dissimilarity (complement of the similarity) between the delta vector and the ground truth position vector are defined as per Equation (5) and Equation (6), respectively. See Figure 2 for a visual explanation.

$$\vec{\mathbf{d}} = \vec{\mathbf{p}} - \hat{\vec{\mathbf{p}}} \quad (5)$$

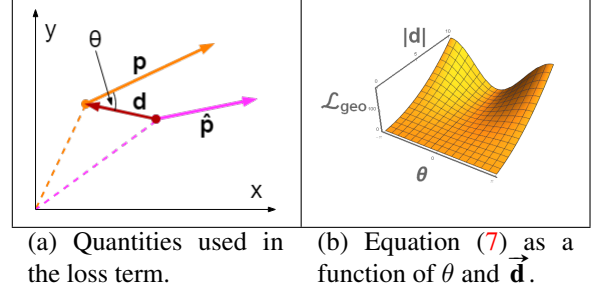


Figure 2: Visualizations of the calculation and behaviour of the loss function in 2D and 3D respectively.

$$\bar{s} = 1 - s = 1 - \cos \theta = 1 - \frac{\hat{\vec{\mathbf{p}}} \cdot \vec{\mathbf{d}}}{\|\hat{\vec{\mathbf{p}}}\| \|\vec{\mathbf{d}}\|} \quad (6)$$

$$\mathcal{L}_{geo} = \|\vec{\mathbf{d}}\|^2 \cdot \bar{s} \quad (7)$$

The loss term \mathcal{L}_{geo} is appended to a pose regression network’s already existing loss function in order to encourage position predictions which align with the ground truth position. The term also encourages alignment (rotational accuracy) between the predicted and ground truth poses.

3.2 Exploring other loss term formulations

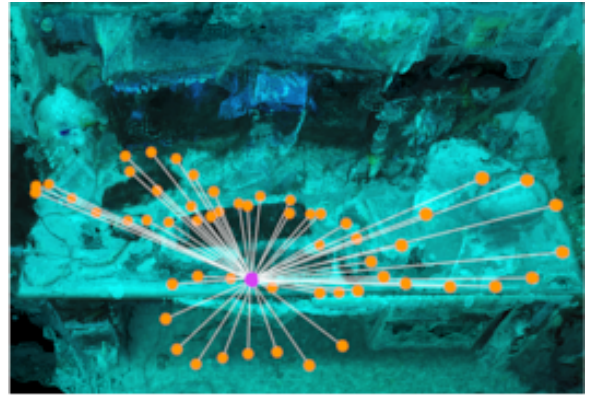


Figure 3: A sample of the predicted pose positions (purple) against the ground truth poses (orange) in the 7Scenes Heads scene using a poorly formulated geometric loss term (Equation (8)). Note that the clustering of the predictions around the origin; the model consistently and incorrectly predicts the position to be near to the origin, which highlights the importance of correctly formulating the loss function. Image best viewed in color.

Since the space of valid geometric loss terms is very large (even before considering hyperparameter choices), experiments were conducted to ensure that the loss term defined

in Equation (7) was fit for the task of informing our training process. A number of different formulations were tested experimentally on the *Chess* scene of the *7Scenes* dataset.

A formulation of interest is the loss term outlined in Equation (8) (variables defined as in Section 3.1). We observe that without scaling the \bar{s} term with the positional error, or without at least including a positional error term, the network regresses positions clustered closely around the scene’s origin (See Figure 3).

$$\mathcal{L}_{alt} = 64 \cdot \bar{s} \quad (8)$$

This formulation encouraged the network to minimize the loss introduced by the dissimilarity term by ensuring the delta vector matched exactly the ground truth vector. Hence the predicted pose was always near to the origin — this behaviour was escaped by introducing a linear dependence on the positional error in the loss function (which can be seen in the final loss function described by Equation (10)). As such, we find that this dependence on the positional error is key in designing powerful geometric loss terms.

Additional experiments were conducted concerning the effect of hyperparameter choices on the performance of the network. Of particular interest is the effect of changing the hyperparameter coefficient for the rotational error. Alterations from 1.5 to 1.2 and from 1.5 to 1.8 decreased median rotational accuracy markedly in each case (decrease of 2.3°). In fact, these changes caused median *positional* accuracy to be increased by 21% and 23% respectively. This suggests that the choice of 1.5 desirably maximizes the median rotational accuracy, hence why this hyperparameter choice appears in the loss function which we use to augment PoseNet and create what will be herein referred to as our *proposed model*.

In short, the final loss term used to train the proposed model (Equation (7)) is the result of an exploration in the space of possible geometric loss terms, and the decisions behind the term’s design were experimentally informed.

4 Experiments

Our experiments are naturally centred around testing the effectiveness of the geometric loss term defined above, with respect to the following criteria:

- **Accuracy:** the system should be able to regress a camera’s pose with a level of positional and rotational accuracy that is competitive with pipelines in the same class. Accuracy is reported using per-scene median positional and rotational error (See Section 5.1).
- **Robustness:** the system should be robust to perceptual aliasing, motion blur and other challenges posed by the datasets (See Section 5.2 and Table 7).

Scene	Extents (metres)	# Train	# Test
Chess	$3 \times 2 \times 1$	4000	2000
Fire	$2.5 \times 1 \times 1$	2000	2000
Heads	$2 \times 0.5 \times 1$	1000	1000
Office (7Scenes)	$2.5 \times 2 \times 1.5$	6000	4000
Pumpkin	$2.5 \times 2 \times 1$	4000	2000
Red Kitchen	$4 \times 3 \times 1.5$	7000	5000
Stairs	$2.5 \times 2 \times 1.5$	2000	1000
Average	-	3714	2429
Office (University)	7×4.5	2196	1099
Meeting	6.5×2	1701	945
Kitchen	6×7	2076	990
Conference	5.5×7.5	1838	949
Coffee Room	6×9	2071	959
Average	-	1976	988
Great Court	95×80	1532	760
King’s College	140×40	1220	343
Old Hospital	50×40	895	182
Shop Facade	35×25	231	103
St Mary’s Church	80×60	1487	530
Street	500×100	3015	2923
Average	-	1397	807

Table 1: The size metrics of the *7Scenes*, *University* and *Cambridge Landmarks* datasets.

- **Time performance:** evaluation should occur in real-time (~ 30 frames per second), such that the system is suitable in hardware limited real-time applications, e.g. on mobile phones (See Section 5.3).
- **Consistency:** performance should be consistent across datasets (See Section 6).

We compare our proposed model with other variations on the same network, particularly considering RGB only pipelines. Another key comparison is the performance of ours and other deep learning pipelines against SIFT based pipelines, or other traditional, feature matching methods.

4.1 Datasets

All pose estimation pipelines are benchmarked against the following three datasets (where data is available), with their recommended train and test splits (See Table 1).

7Scenes [15]. 7 indoor locations in a domestic office context. The dataset features large training and testing sets (in the thousands). The camera path moves continuously through the scene in order to gather images in distinct sequences.



Chess Fire Heads Office Pumpkin Red Kitchen Stairs

Table 2: Sample images from each of the 7 scenes in the *7Scenes* dataset.



Great Court Kings College Old Hospital Shop Facade St Mary's Church Street

Table 3: Sample images from each of the 6 scenes in the *Cambridge Landmarks* dataset.



Office Meeting Kitchen Conference Coffee Room

Table 4: Sample images from each of the 5 scenes in the *University* dataset.

Images include motion blur, featureless spaces and specular reflections (See Table 7), making this a challenging dataset, and one that has been used prolifically in the camera relocalization literature. The ground truths poses are gathered with KinectFusion, and the RGBD frames have a resolution of 640×480 px.

Cambridge Landmarks [4, 2, 3]. 6 outdoor locations in and around Cambridge, The United Kingdom. The larger spatial extent and restricted data size make this a challenging dataset to learn to regress pose from — methods akin to the one presented in this work typically only deliver positional accuracy in the scale of metres (see Table 5). In the context of *domestic* robotics and other indoor applications, the results against this benchmark are less important, but the dataset does provide a common point of comparison, and also features large expanses of textureless surfaces. Ground truth poses are generated by a SfM process.

University [5]. 5 indoor scenes in a university context. Ground truth poses are gathered using odometry estimates and “manually generated location constraints in a pose-graph optimization framework” [5]. The dataset, similarly to *7Scenes*, includes challenging frames with high degrees of perceptual aliasing, where multiple frames (with different poses) give rise to similar images [21]. Although the scenes are registered to a common coordinate system in the *University* dataset and thus a network can be trained on the full dataset, we choose to train and test our model scene-wise for consistency.

4.2 Architecture and training

As stated, we primarily experiment with the PoseNet architecture. For the purpose of brevity we redirect the reader to

the original publication [4], as here we only describe crucial elements of the network’s design and operation.

The PoseNet architecture is in itself based on the GoogLeNet architecture [17], a 22 layer deep network which performs classification and detection. The design of PoseNet leverages the notion that regressing pose from images will require feature extraction, and thus only the final three softmax classifiers need to be replaced with affine regressors, which output pose using translation (vector coordinates) and rotation (quaternion coefficients). The network is pretrained using large classification datasets such as *Places* [22].

We build on a TensorFlow implementation of PoseNet [16] whose original loss function is defined in Equation (9). This loss function is updated to that of Equation (10) for the purpose of our experiments. We label the i^{th} affine regressor’s hyperparameters using α_i and β_i and denote position, rotation, dissimilarity and the delta vector using \vec{p} , \vec{q} , \vec{s} and \vec{d} respectively.

Rotation is encoded using quaternions, since the space of rotations is continuous, and results can be easily normalized to the unit sphere in order to ensure valid rotations.

All three affine regressor predictions are used in calculating loss, but each have different hyperparameter weightings: $\alpha_1 = \alpha_2 = 0.3$, $\alpha_3 = 1$, $\beta_1 = \beta_2 = 150$ and $\beta_3 = 500$. We keep these hyperparameter values, but increase the weighting of the angular component (as we find this provides the most well rounded results, see Section 3.2). The combined translational error amongst the affine regressors is removed in favor for the magnitude of the delta vector, which still represents the positional error.

$$\mathcal{L}_{original} = \alpha_i \cdot \|\hat{\vec{p}}_i - \vec{p}\| + \beta_i \cdot \|\hat{\vec{q}}_i - \vec{q}\| \quad (9)$$

$$\mathcal{L}_{proposed} = 1.5 \cdot \beta_i \cdot \|\hat{\vec{q}}_i - \vec{q}\| + \|\vec{d}\| + \|\vec{d}\|^2 \cdot \bar{s} \quad (10)$$

In order to demonstrate the consistency and generalization of the proposed network, we train against all scenes in all datasets using the same setup. Each model is trained per-scene over 300,000 iterations with a batch size of 75 on a Tesla K40c, which takes ~ 10 hours to complete.

5 Results

We present the results of our proposed model and provide a comparison of other versions of PoseNet in Table 5 and Table 8. A brief discussion of our system’s performance regarding the criteria outlined in Section 4 follows.

5.1 Accuracy

It is observed that the proposed model outperforms the default version of PoseNet in some scenes — particularly the *Stairs* scene. In the *Stairs* scene, repetitious structures, e.g. staircases, make localization harder, yet the proposed model is robust to such challenges. The network is outperformed in others scenes; namely outdoor datasets with large spatial extents, but in general, performance is improved for the indoor datasets *7Scenes* and *University*.

A set of cumulative histograms for some of the evaluated scenes are provided in Table 6. We compare the distribution of the positional error and rotational error for the default PoseNet and for our proposed model. Median values (provided in Table 5 and Table 8) are plotted for reference.

We note that the proposed model’s errors are strictly less than the default PoseNet’s throughout the majority of the *Chess* and *Coffee Room* distributions. The default PoseNet outperforms our proposed model with respect to rotational accuracy in the $10^\circ - 30^\circ$ range in the *Coffee Room* scene.

Note the lessened performance observed from the proposed model on the *King’s College* scene; where the positional errors distributions for the two networks are nearly aligned. Moreover, the default PoseNet more accurately regresses rotation in this outdoor scene. See Section 5.2 and Section 6 for further discussion.

5.2 Robustness

The robustness of our system to challenging test frames — that is, images with motion blur, repeated structures or demonstrating perceptual aliasing [6] — can be determined via the cumulative histograms in Table 6. For the purpose of visualization some difficult testing images from the *7Scenes* dataset are displayed in Table 7.

The hardest frames in the test set by definition produce the greatest errors. Consider the positional error for the *Meeting* scene: our proposed model reaches a value of 1.0 on the y-axis before the default PoseNet does, meaning that the *hardest* frames in the test set have their position regressed more accurately. This analysis extends to each of the cumulative histograms in Table 6, thus confirming our proposed loss function’s robustness to difficult test scenarios, as the frames of greatest error consistently have less than or comparable errors to that of default PoseNet.

5.3 Efficiency

Training time. The duration of the training stage compared between our implementation and default PoseNet is by design, very similar, and highly competitive when compared to the other systems analyzed in Table 5. This is due to the relatively inexpensive computing cost of introducing a *simple* geometric loss term into the network’s overall loss function. The average training time for default PoseNet and for our augmented PoseNet over the *University* dataset is 10 : 21 : 31 and 10 : 23 : 33 respectively (HH:MM:SS), where both tests are ran on the same hardware.

Testing time. The network operation during the test time is naturally not affected by the loss function augmentation. The time performance when testing is similar to that of the default PoseNet and in general is competitive amongst camera relocalization pipelines. We observe a total elapsed time of 16.04 seconds when evaluating the entire *Coffee Room* scene testing set, whereas it takes 16.03 seconds using the default PoseNet. In other words, both systems take ~ 16.8 ms to complete a single inference on our hardware.

Memory cost. Memory cost in general for CNNs is low — only the weights for the trained layers and the input image need to be loaded into memory. When compared to feature matching techniques, which need to store feature vectors for all instances in the test set, or SIFT-based matching methods with large memory and computational overheads, CNN approaches in general appear desirable — especially in resource constrained environments. Both the proposed model and the default PoseNet take 8015MiB and 10947MiB to train and test respectively (as reported by *nvidia-smi*). For interest, the network weights for the proposed model’s TensorFlow implementation total only 200MB.

6 Discussion and future work

Experimental results confirm that the loss term used to augment PoseNet has a positive impact on robustness and accuracy, whilst maintaining time and memory performance (during both training and testing). The proposed model could still be improved with regards to its relative accuracy com-

Scene	Active Search [12]	Geometric PoseNet [3]	LSTM PoseNet [19]	Bayesian PoseNet [2]	Default PoseNet [4]	Proposed model
Chess	0.04m, 1.96°	0.13m, 4.48°	0.24m, 5.77°	0.37m, 7.24°	0.32m, 8.12°	0.31m, 7.04°
Fire	0.03m, 1.53°	0.27m, 11.3°	0.34m, 11.9°	0.43m, 13.7°	0.47m, 14.4°	0.49m, 13.3°
Heads	0.02m, 1.45°	0.17m, 13.0°	0.21m, 13.7°	0.31m, 12.0°	0.29m, 12.0°	0.24m, 15.7°
Office (7Scenes)	0.09m, 3.61°	0.19m, 5.55°	0.30m, 8.08°	0.48m, 8.04°	0.48m, 7.68°	0.40m, 10.0°
Pumpkin	0.08m, 3.10°	0.26m, 4.75°	0.33m, 7.00°	0.61m, 7.07°	0.47m, 8.42°	0.49m, 9.50°
Red Kitchen	0.07m, 3.37°	0.23m, 5.35°	0.37m, 8.83°	0.58m, 7.54°	0.58m, 11.3°	0.53m, 7.98°
Stairs	0.03m, 2.22°	0.35m, 12.4°	0.40m, 13.7°	0.48m, 13.1°	0.56m, 15.4°	0.48m, 14.7°
Average	0.05m, 2.46°	0.23m, 8.12°	0.31m, 9.85°	0.47m, 9.81°	0.45m, 11.0°	0.42m, 11.2°
Great Court	—	6.83m, 3.47°	—	—	—	—
Street	0.85m, 0.83°	20.3m, 25.5°	—	—	3.67m, 6.50°	—
King’s College	0.42m, 0.55°	0.88m, 1.04°	0.99m, 3.65°	1.74m, 4.06°	1.92m, 5.40°	2.28m, 4.05°
Old Hospital	0.44m, 1.01°	3.20m, 3.29°	1.51m, 4.29°	2.57m, 5.14°	2.31m, 5.38°	3.90m, 8.75°
Shop Facade	0.12m, 0.40°	0.88m, 3.78°	1.18m, 7.44°	1.25m, 7.54°	1.46m, 8.08°	2.48m, 10.2°
St Mary’s Church	0.19m, 0.54°	1.57m, 3.32°	1.52m, 6.68°	2.11m, 8.38°	2.65m, 8.48°	3.02m, 7.79°
Average ¹	0.29m, 0.63°	1.63m, 2.86°	1.30m, 5.52°	1.92m, 6.28°	2.09m, 6.84°	2.92m, 7.70°

Table 5: The results of various camera localization methods for the 7Scenes and Cambridge Landmarks datasets. Similar classes of systems are grouped (left to right: SIFT-based, augmented architecture networks and other networks). The lowest errors of each group are emboldened. Note that our contribution is competitive with systems in the same class in *indoor* datasets with respect to median positional error.

¹ Average calculated using only the scenes: *King’s College*, *Old Hospital*, *Shop Facade* & *St Mary’s Church* as full dataset performance is not available for all pipelines.

² For cells where results could not be procured (due to implementation availability or otherwise), a ‘—’ is used. The inclusion of such results would not greatly effect any conclusion on the performance of the systems, particularly with respect to the *Street* scene, as its large spatial extents only reduce the consistency of the Cambridge Landmarks dataset.

pared to other pipelines, but such pipelines demonstrate that an increase in accuracy comes at the expense of time performance.

Scene	Default PoseNet [4]	Proposed model
Office (University)	1.05m, 16.2°	0.91m, 11.0°
Meeting	1.78m, 10.1°	1.30m, 9.58°
Kitchen	1.19m, 12.5°	1.25m, 15.5°
Conference	2.88m, 13.3°	2.83m, 15.8°
Coffee Room	1.41m, 14.9°	1.21m, 13.3°
Average	1.66m, 13.4°	1.50m, 13.0°

Table 8: A study on the direct effects of using our proposed loss function, instead of the default loss function for PoseNet. The lowest errors of each group are emboldened. Note that our contribution majorly outperforms the default PoseNet in both median positional and median rotational error throughout the University dataset.

For example, the proposed model *is* outperformed by competitors which use more expensive reprojection methods [3], but these procedures infringe on the default PoseNet’s ease-of-training.

The network is also outperformed by the SIFT-based image localization algorithm ‘Active Search’ [12], indicating that there is still some work required until the gap between SIFT-based algorithms and CNNs is closed (in the context of RGB-only image localization). However, SIFT localization operates on a much longer timescale, and can be highly computationally expensive depending on the dataset and pipeline being used [20].

In a similar vein, the proposed model is outperformed by PoseNet augmented with LSTMs [19] — a more computationally expensive approach — though it should be noted that our approaches are not necessarily mutually exclusive, and LSTMs with augmented loss functions is perhaps an avenue for future research.

Ultimately, the loss function augmentation described in this work illustrates that intuitive loss terms, designed with respect to a specific task (in this case image localization) can positively impact the performance of deep networks.

As an aside, we note a discrepancy in the consistency of our model between datasets with differing spatial extents. It is suspected that further hyperparameter tuning is required in order to allow the \mathcal{L}_{geo} term (Equation (7)) to balance better with the default positional and rotational loss terms (Equation (9)).

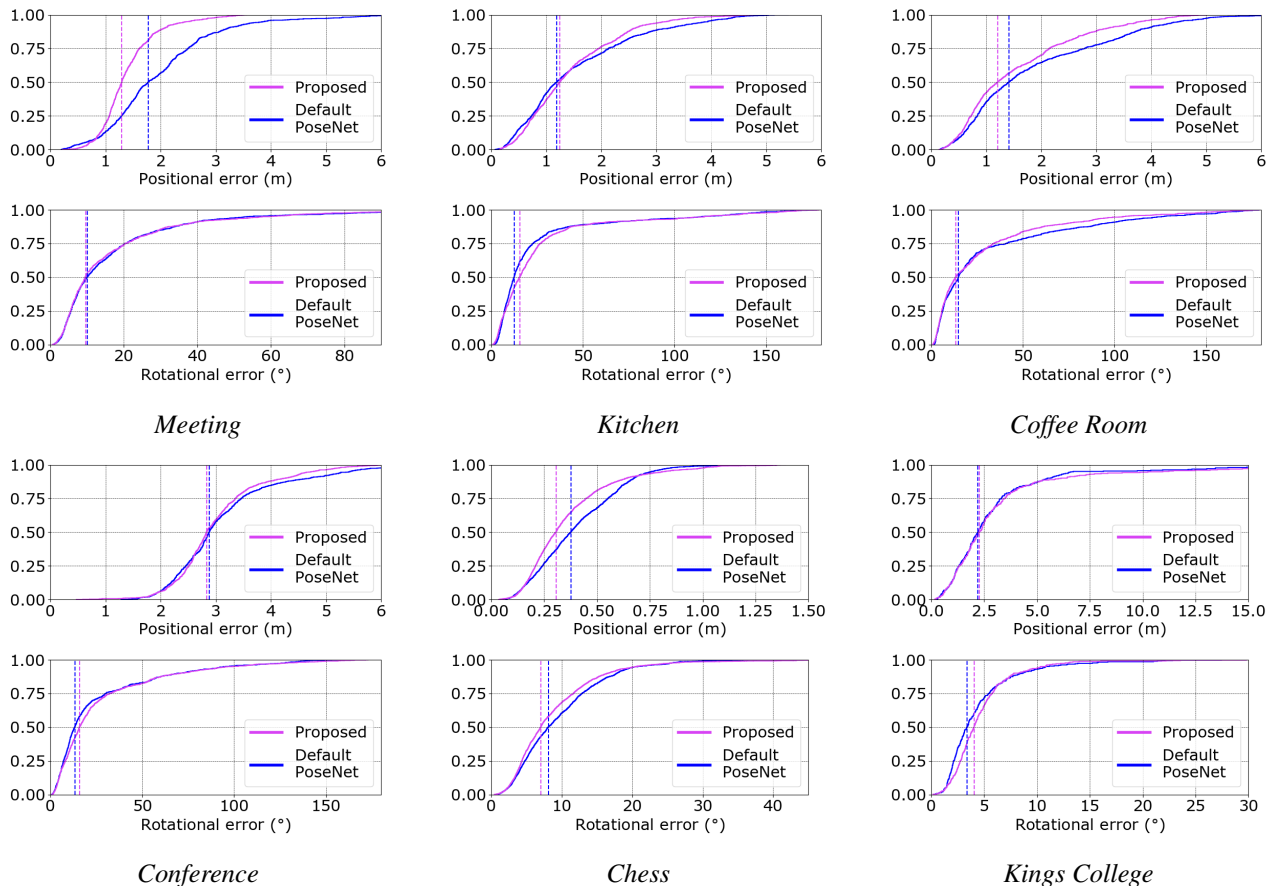


Table 6: Cumulative histograms of positional and rotational errors, with median values plotted as a dotted line. Note that the proposed model’s positional error distribution is strictly less than (shifted to the left of) the default PoseNet’s positional error distribution for the indoor scenes (except *Conference*, where performance is comparable). Additionally, the maximum error of the proposed model is lower in the scenes *Meeting*, *Coffee Room* and *Kitchen*, meaning that our implementation is robust to some of the most difficult frames offered by the University dataset. Images best viewed in colour.



(a) Motion blur (b) Repeated structures (c) Textureless & reflective surfaces

Table 7: (a) - (c) Images from the 7Scenes dataset where accurately regressing pose is challenging.

This would suggest that the loss term introduces a dependency on the average scene geometry, but more investigation is required in order to provide a meaningful discussion of these results. We leave this investigation up to future work.

7 Conclusion

In summary, the effects of adding a geometric loss term to an existing pose regression network are investigated, and the performance of such a system is compared to other similar systems across common image localization benchmarks. Improvements to performance in the image localization task are observed, without any drastic increase in evaluation speed or training time. Particularly, the median positional accuracy is — on average — increased for indoor datasets when compared to a version of the model without the suggested loss term.

This work suggests that the simple Euclidean distance between the ground truth and the regressed vectors, although often used as a measure of loss for many neural networks, can be improved upon. Specifically, loss functions designed with the primary goal of the network in mind may yield better performing models. For pose regression networks, the

distinct nature of positional and rotational quantities, and how to combine these terms to best inform a network’s loss function, warrants future research.

References

- [1] E. Brachmann and C. Rother. Learning less is more - 6d camera localization via 3d surface regression. *CoRR*, abs/1711.10228, 2017. [2](#)
- [2] A. Kendall and R. Cipolla. Modelling uncertainty in deep learning for camera relocalization. *CoRR*, abs/1509.05909, 2015. [2](#), [5](#), [7](#)
- [3] A. Kendall and R. Cipolla. Geometric Loss Functions for Camera Pose Regression with Deep Learning. *arXiv:1704.00390 [cs]*, Apr. 2017. arXiv: 1704.00390. [2](#), [5](#), [7](#)
- [4] A. Kendall, M. Grimes, and R. Cipolla. PoseNet: A Convolutional Network for Real-Time 6-DOF Camera Relocalization. *arXiv:1505.07427 [cs]*, May 2015. arXiv: 1505.07427. [1](#), [2](#), [5](#), [7](#)
- [5] Z. Laskar, I. Melekhov, S. Kalia, and J. Kannala. Camera relocalization by computing pairwise relative poses using convolutional neural network. *arXiv preprint arXiv:1707.09733*, 2017. [2](#), [5](#)
- [6] X. Li, J. Ylioinas, and J. Kannala. Full-frame scene coordinate regression for image-based localization. *CoRR*, abs/1802.03237, 2018. [6](#)
- [7] D. Massiceti, A. Krull, E. Brachmann, C. Rother, and P. H. S. Torr. Random forests versus neural networks - what’s best for camera relocalization? *CoRR*, abs/1609.05797, 2016. [2](#)
- [8] I. Melekhov, J. Kannala, and E. Rahtu. Relative camera pose estimation using convolutional neural networks. *CoRR*, abs/1702.01381, 2017. [2](#)
- [9] I. Melekhov, J. Ylioinas, J. Kannala, and E. Rahtu. Image-based localization using hourglass networks. *CoRR*, abs/1703.07971, 2017. [2](#)
- [10] P. Purkait, C. Zhao, and C. Zach. Spp-net: Deep absolute pose regression with synthetic views. *CoRR*, abs/1712.03452, 2017. [2](#)
- [11] N. Radwan, A. Valada, and W. Burgard. Vlocnet++: Deep multitask learning for semantic visual localization and odometry. *CoRR*, abs/1804.08366, 2018. [2](#)
- [12] T. Sattler, B. Leibe, and L. Kobbelt. Efficient and effective prioritized matching for large-scale image-based localization. *IEEE Transactions on Pattern Analysis and Machine Intelligence*, 39(09):1744–1756, sep 2017. [1](#), [2](#), [7](#)
- [13] J. L. Schönberger, E. Zheng, J.-M. Frahm, and M. Pollefeys. Pixelwise view selection for unstructured multi-view stereo. In *ECCV*, 2016. [2](#)
- [14] J. L. Schnberger and J. Frahm. Structure-from-motion revisited. In *2016 IEEE Conference on Computer Vision and Pattern Recognition (CVPR)*, pages 4104–4113, June 2016. [2](#)
- [15] J. Shotton, B. Glocker, C. Zach, S. Izadi, A. Criminisi, and A. Fitzgibbon. Scene coordinate regression forests for camera relocalization in rgb-d images. *IEEE Conference on Computer Vision and Pattern Recognition (CVPR)*, pages 2930–2937, 2013. [4](#)
- [16] K. Sommer. Tensorflow posenet implementation. <https://github.com/kentsommer/tensorflow-posenet>. Accessed: 01-02-2019. [5](#)
- [17] C. Szegedy, W. Liu, Y. Jia, P. Sermanet, S. E. Reed, D. Anguelov, D. Erhan, V. Vanhoucke, and A. Rabinovich. Going deeper with convolutions. *CoRR*, abs/1409.4842, 2014. [5](#)
- [18] A. Valada, N. Radwan, and W. Burgard. Deep auxiliary learning for visual localization and odometry. *CoRR*, abs/1803.03642, 2018. [2](#)
- [19] F. Walch, C. Hazirbas, L. Leal-Taix, T. Sattler, S. Hilsenbeck, and D. Cremers. Image-based localization using LSTMs for structured feature correlation. *arXiv:1611.07890 [cs]*, Nov. 2016. arXiv: 1611.07890. [2](#), [7](#)
- [20] C. Wu. Towards linear-time incremental structure from motion. In *2013 International Conference on 3D Vision - 3DV 2013*, pages 127–134, June 2013. [7](#)
- [21] L. Zaval and T. M. Gureckis. The impact of perceptual aliasing on exploration and learning in a dynamic decision making task. In *Proceedings of the Annual Meeting of the Cognitive Science Society*, 2010. [5](#)
- [22] B. Zhou, A. Lapedriza, J. Xiao, A. Torralba, and A. Oliva. Learning deep features for scene recognition using places database. In Z. Ghahramani, M. Welling, C. Cortes, N. D. Lawrence, and K. Q. Weinberger, editors, *Advances in Neural Information Processing Systems 27*, pages 487–495. Curran Associates, Inc., 2014. [5](#)